IEEE Photonics Journal
An IEEE Photonics Society Publication

Invited Paper

Compact Optical Switches and Modulators Based on Dispersion Engineered Photonic Crystals

Volume 2, Number 3, June 2010

Liam O'Faolain
Daryl M. Beggs
Thomas P. White
Tobias Kampfrath
Kobus Kuipers
Thomas F. Krauss

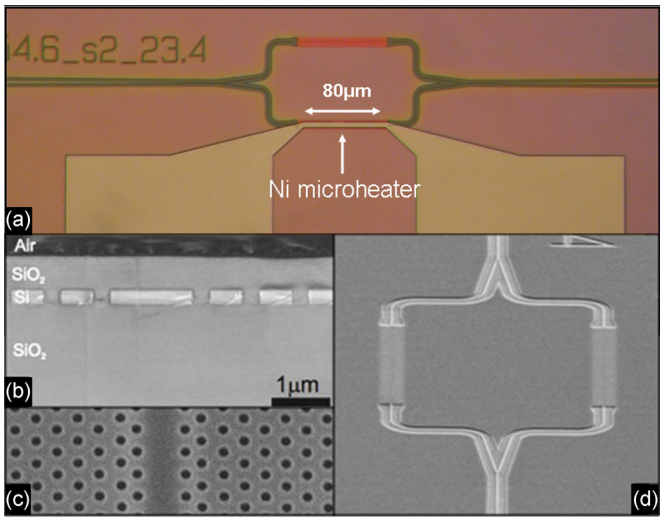

DOI: 10.1109/JPHOT.2010.2047918
1943-0655/$26.00 ©2010 IEEE

Compact Optical Switches and Modulators Based on Dispersion Engineered Photonic Crystals

Liam O'Faolain,[1] Daryl M. Beggs,[1] Thomas P. White,[1] Tobias Kampfrath,[2] Kobus Kuipers,[2] and Thomas F. Krauss[1]

(Invited Paper)

[1]School of Physics and Astronomy, University of St. Andrews, St. Andrews KY16 9SS, U.K.
[2]FOM Institute AMOLF, 1098 XG Amsterdam, The Netherlands

DOI: 10.1109/JPHOT.2010.2047918
1943-0655/$26.00 ©2010 IEEE

Manuscript received March 17, 2010; accepted March 27, 2010. First published Online April 12, 2010. Current version published June 1, 2010. This work was supported through the European Union FP6-FET "SPLASH" and UK EPSRC Silicon Photonics projects. This work is also part of the research program of FOM, which is financially supported by the NWO. This paper was presented in part at the 2009 IEEE Photonics Society Annual Meeting. Corresponding author: L. O'Faolain (e-mail: jww1@st-andrews.ac.uk).

Abstract: We use slow-light photonic crystals to enhance optical switching and modulation in silicon. By using dispersion-engineered designs, a switch as short as 5 μm was achieved, in which we have demonstrated rerouting of optical pulses on a 3-ps time scale through the absorption of a femtosecond pulse. We additionally demonstrate a modulator with a Mach–Zehnder interferometer (MZI) configuration with flat-band slow-light photonic crystal phase shifters that is designed to give a large group-index–bandwidth product. An extinction ratio in excess of 15 dB is obtained over the entire 11-nm bandwidth of the modulator.

Index Terms: Engineered photonic nanostructures, ultrafast nonlinear processes, nonlinear effects, slow light, silicon nanophotonics, photonic crystals.

1. Introduction

Optical switches and modulators are key components in next-generation communications technologies. Future terabit-per-second telecommunications networks will need to operate all-optically, avoiding the bottleneck of electro-optic conversion that is currently required for signal rerouting. Electrical interconnects in massively parallel multiple-core computer chips would consume excessive amounts of power, making on-chip optical communication an increasingly attractive alternative. Cheap, reliable, and compact on-chip optical switches and modulators are key prerequisites for these technologies. CMOS compatibility is another important concern requiring their fabrication in silicon [1]–[9].

In III–V semiconductor systems and Lithium Niobate, large electro-optic coefficients effects are available, making optical switching an "easy" operation. However, in silicon, the corresponding nonlinear effects and refractive index changes are weak or small, with the result that switches tend to be either very long or require high powers to operate [4].

The use of resonant enhancement is one means of increasing the sensitivity of light to the small changes in refractive index available [3]. However, using the modes of a cavity tends to strongly limit the bandwidth of the device and make it very sensitive to fabrication imperfections [10]. Slow light is a resonant effect that is created in periodic structures, such as photonic crystals. When the

Bragg condition is satisfied, a standing wave is formed and the device acts as a high-reflectivity mirror. Away from this condition, light coherently scattered by these mirror planes interferes with the incoming light, forming an interference pattern that moves forward slowly. This effect is known as slow light and may be used to enhance the refractive index change while preserving bandwidth.

To switch or reroute light, a π phase change is required between two optical paths or modes, encapsulated in the equation $\Delta kL = \pi$, where L is the switching length, and Δk is the change in wave vector between the two paths/modes brought about by the actuator. To reduce L, it is desirable to design a device in which the Δk is large, even for small refractive index changes. Such a condition is provided by a slow-light region [11].

Here, we describe two slow-light-enhanced optical devices: an optical modulator and an optical switch. The modulator is described in Section 3 and consists of a symmetric Mach–Zehnder interferometer (MZI) with slow-light dispersion-engineered photonic crystal waveguides comprising each arm. Switching is demonstrated using the thermo-optic effect. The MZI geometry naturally provides a large operating bandwidth, but resonant enhancements tend to reduce this. However, when designed to have a large group-index–bandwidth product, the photonic crystal phase shifter can provide modulation over an appreciable bandwidths—here, we demonstrate 11 nm. The optical switch described in Section 4 is based on two closely spaced photonic crystal waveguides in a directional coupler geometry [9]. We have previously demonstrated switching using the thermo-optic effect with a time scale of 20 μs [12]. Here, we report on a similar switch that uses the free-carrier effect to modulate the refractive index of the silicon (cf. [13]). Using a pump–probe experimental setup, we demonstrate switching times as short as 3 ps [14], [15], and we show that this time is not limited by the time of flight of the pulse (which has a subpicosecond time scale). On the contrary, the switch is bandwidth limited, meaning that a faster switching time can only be demonstrated with a shorter pulse. To support these pulses, more bandwidth is required than is available with this particular device.

We present two different device geometries—MZI modulator and directional coupler—each with their own advantages. The MZI geometry allows a tradeoff between the length and the phase shift, which is important in silicon where fast effects, such as carrier depletion [16] provide only small refractive index modulations. The directional coupler geometry provides a strong interaction and therefore a very short length, allowing for more densely integrated circuitry. Additionally (and more importantly for future terahertz networks), the shorter pulse transit times through the device allows potentially faster operation and lower switching energies. The nature of the slow-light enhancement in the MZI typically offers a bandwidth of $\approx$ 5–15 nm, while the PhC directional coupler is limited to around $\approx$1 nm. This broad bandwidth of the MZI provides stability against temperature fluctuations (important for on-chip applications), which is more difficult to achieve in the directional coupler geometry (possibly requiring active compensation).

2. Dispersion Engineering

A silicon photonic crystal slab consists of a regular lattice of holes etched into a thin silicon membrane. By removing a single row of holes from the bulk PhC a waveguide known as a W1 is formed. This waveguide guides light through two effects: 1) $\sim$index guiding, due to the reduced average refractive index in the adjacent regions, and 2) $\sim$band-gap guiding, where light is reflected by the photonic band gap of the photonic crystal (acting as a Bragg mirror) and can support a single mode of even symmetry at frequencies within the band gap of the photonic crystal. In the vertical direction, light confinement is provided by total internal reflection.

The dispersion (k, ω) of the fundamental waveguide mode is shown in Fig. 1(a). The group velocity is given by its slope: $v_g = d\omega/dk$. The simulated and experimental (measured using the technique of [17]) group index is shown in Fig. 1(b) for three different lengths of W1 (20 μm, 30 μm, and 80 μm). There is excellent agreement between calculation and experiment, even for group indices in excess of 100, which is testament to the quality of the fabrication. As can be seen in Fig. 1(b), the group velocity dispersion is high, resulting in rapid temporal broadening of any pulse. A region in which the GVD is close to zero and is known as "flat-band slow light" is preferable for most applications. The group-index–bandwidth product [10] is the key figure of merit used to

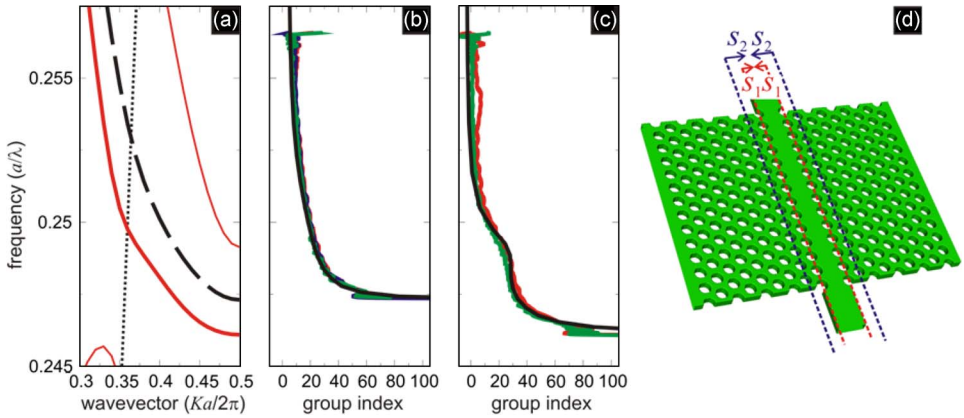

Fig. 1. (a) Dispersion relation of photonic crystal slab waveguides with a silica cladding. The W1 waveguide mode is shown by the dashed line, and a dispersion engineered PhCW is shown in red, with the lightline of the silica cladding given by the dotted line. (b) The calculated (black line) and measured (red, green, and blue lines) group index spectra for the W1 waveguide. (c) Calculated (black) and measured (red, green, and blue lines) group index spectra for the dispersion engineered PhCW. (d) Schematic of the W1 photonic crystal slab waveguide. The mechanism of dispersion engineering, laterally shifting of the first (S1) and second rows of holes (S2), is also shown.

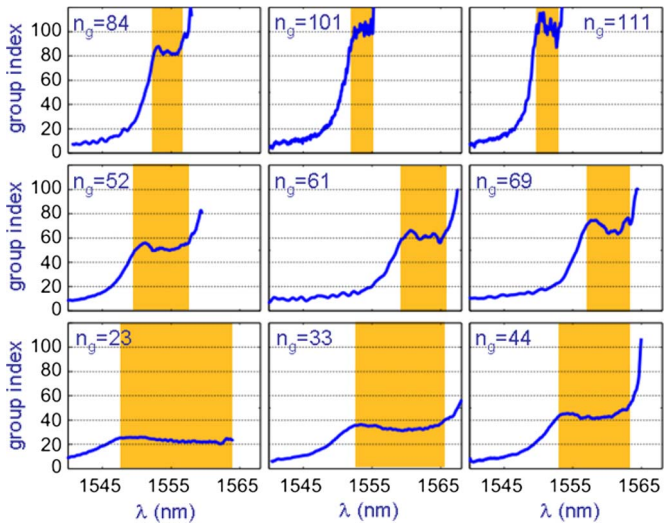

Fig. 2. Group index measurements of photonic crystal waveguides that have been designed to have regions of flat-band slow light of constant group-index–bandwidth products at differing group indices (indicated). The shaded bars represent the wavelength range within which the group index varies by less than 10%.

quantify the performance of these devices. There are now a number of dispersion-engineering methods available to achieve flat band slow light in photonic crystals. These range from altering the width of the waveguide [18]–[21] to changing the diameter of the holes near the defect [22], [23] to dispersion compensating structures [24]. A detailed discussion of these techniques and their relative merits is given in [10]. Here, we have used the method of laterally shifting the first and second rows of holes adjacent to the defect [20]; see Fig. 1(d). This scheme avoids the need for nanometer control the hole size, which is challenging [25], and instead uses nanometer control of the hole position, which plays to the strengths of electron-beam lithography.

Systematically scanning the parameters s_1 and s_2 in simulation or experiment provides a means of designing waveguides with high group-index–bandwidth products. At the desired group index,

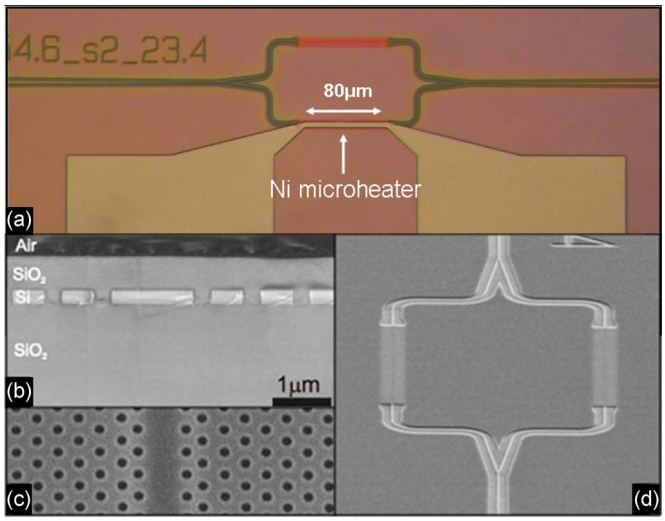

Fig. 3. Fabrication of the photonic crystal Mach–Zehnder modulator. (a) Optical micrograph of the finished device. The short PhC phase shifters (80 μm) can be seen in each arm of the MZI. The nickel microheater and electrical contact pads are also visible. (b) SEM micrograph of the cross section of the oxide clad PhC, with the infilling of the holes clearly demonstrated. (c) Closeup of the waveguide. The lateral shifting of the first and second row of holes can be seen (d) Overview of the complete Mach–Zehnder (prior to oxide cladding and contact deposition).

the s_1 and s_2 values that maximize this product should be selected. Fig. 2 shows the measured group indices for a selection of devices. The flat-band slow-light regions are indicated by the shaded bands, with the group index defined as "constant" if it varies by less than 10% throughout the entire band. In all these instances, the normalized group-index–bandwidth product is approximately 0.3, demonstrating the fundamental tradeoff between group index and bandwidth.

3. Photonic Crystal Modulator

3.1. Modulator Design and Fabrication

To achieve broad bandwidth switching, we placed dispersion-engineered photonic crystal waveguides in each arm of a symmetric MZI, as shown in Fig. 3. The phase shift is provided via the thermo-optic tuning of one of the arms by means of an integrated microheater. Following the above procedure, the PhCWs are designed to have a constant group index of 28 over a bandwidth of approximately 13 nm. The entire structure is clad with silica [the cross section is presented in Fig. 3(b)], which, although reducing the index contrast, improves the CMOS compatibility. It also provides a spacer layer to isolate the optical mode from the lossy metal of the microheaters. The reduced refractive index contrast introduces some additional design limitations, slightly reducing the group indices achievable relative to air-bridge versions, but crucially, the loss per unit delay figure of merit (introduced in [10]) is not increased [26]. Mode conversion interfaces, which are described in [10], have also been included to aid coupling.

The fabrication closely follows that of [20] (c.f. the fabrication of the switch in [12]). A SOITEC silicon-on-insulator wafer with 220 nm of silicon on a 2-μm-thick buried oxide layer is spun with 400-nm layer of ZEP-520A (Zeon Chemicals). The ZEP-520A is patterned with the MZI and PhC designs using electron-beam lithography, and this pattern is transferred to the silicon layer by reactive ion etching with a SF_6/CHF_3 gas mixture. The holes making up the PhC waveguide and the MZI design can be seen in Fig. 3(c) and (d), respectively. A silica cladding is then deposited using the spin-on-glass FOx-14 (commercially available from Dow-Corning), which leaves a 600-nm layer after hard-baking at 400 °C for 3 h. An integrated nickel microheater, consisting of 5-μm-wide, 8-nm-thick strips of nickel, is then added over one of the PhC phase shifters using a

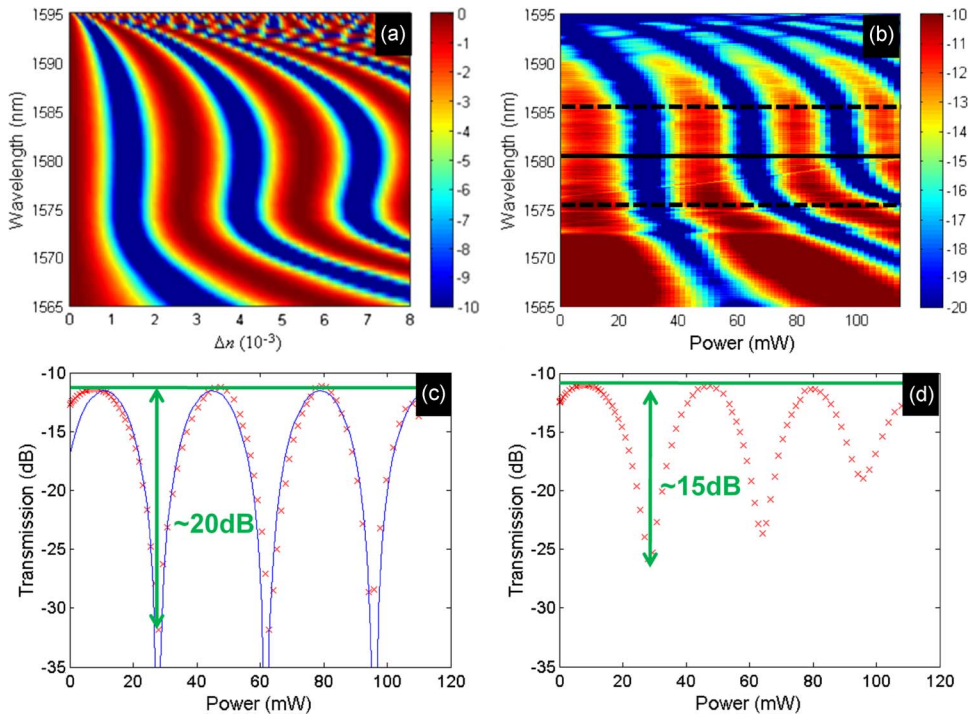

Fig. 4. (a) Theoretical transmission spectra of MZI modulator as a function of n, which is the change of refractive index of the silicon in one of the PhC phase shifters. The color bar gives the transmission in decibels. (b) Measured transmission spectra of MZI modulator as a function of the electrical power delivered to the integrated microheater. The dashed lines represent the limits of the 11-nm bandwidth, which is defined by the spectral region of flat-band slow light in the dispersion engineered PhC phase shifters. The color bar gives the transmission in decibels. (c) Measured (red crosses) and calculated (blue lines) transmission as a function of electrical power delivered to the microheater at a wavelength of 1581 nm, as marked by the solid line in (b). (d) Average transmission over the 11-nm bandwidth as indicated by the dashed lines in (b).

photolithography, evaporation deposition, and lift-off procedure. A micrograph of the final device is shown in Fig. 3(a).

As silicon has a thermo-optic coefficient of $dn/dT = 1.8 \times 10^{-4}$ K^{-1}, its refractive index increases with temperature. When the microheater is on, the dispersion curve of the photonic crystal waveguide mode is shifted to lower frequencies, changing the k-vector and thus inducing a phase shift between the two arms. When this phase shift ΔkL reaches a value of π, the light propagating in each arm of the MZI destructively interferes at the output, switching the device to its off state. The slow-light enhancement is now apparent—a greater phase shift per unit length of the waveguide is achieved, allowing the physical length of the device to be reduced (whereas the optical length is constant).

When heat is applied, the shift in wave vector is given by $\Delta k = \Delta n \omega_0 S$, where $S = n_g/n$ is the slowdown factor, Δn is the change of refractive index, and ω_0 is the frequency. The length required for the π phase shift is reduced by a factor S. To give figures for the example shown here, a phase-shifter that is 80 μm long is required to operate with an index change of approximately 10^{-3}.

3.2. Modulator Performance

Using an end-fire characterization setup, light from a broadband (1520–1620 nm) amplified spontaneous emission (ASE) source was passed through a polarizing beam splitter cube, selecting only the transverse electric (TE) polarization (electric field in the plane of the silicon slab) and coupled to the modulator chip. Needle probes were used to contact the microheaters, and the transmitted light analyzed using an optical spectrum analyzer (OSA) as function of the electrical power delivered to the heater. The results are shown in Fig. 4.

TABLE 1
Comparison of silicon optical MZI modulators

	Liu *et al.* [4]	Vlasov *et al.* [28]	Green *et al.* [7]	Chen *et al.* [29]	This work
Modulation	Electro-optic	Thermo-optic	Electro-optic	Electro-optic	Thermo-optic
Extinction (low freq)	~20 dB	~20 dB	6-10 dB	10 dB	20 dB
Δn	$\sim 0.9 \times 10^{-4}$	$\sim 2 \times 10^{-4}$	4×10^{-3}	$\sim 1.2 \times 10^{-4}$	$1 - 2 \times 10^{-3}$
Length	3 mm	250 μm	200 μm	300 μm	80 μm
Optical bandwidth	> 75 nm	< 0.5 nm	> 50 nm	< 3 nm	~10 nm
Maximum Modulation Speed	30 GHz	10 MHz	10 GHz	1.6 GHz	~50 KHz [12]

In Fig. 4(a) and (b), the theoretical and measured transmission spectra are shown as a function of the refractive index change Δn of the PhC phase shifter (theoretical) or the electrical power delivered to the microheater (experimental). The color bar shows the transmission in decibels covering a range of 10 dB. With the conversion from power to refractive index change, there is good qualitative agreement between the experimental measurements and the simulations.

Fig. 4(c) shows the transmission at a wavelength in the middle of the flat-band slow-light region [1581 nm, shown by the solid line in (b)] as a function of the thermal heating. It should be noted that the first peak in transmission occurs at a power of approximately 9 mW, indicating that the MZI is initially slightly unbalanced. This unbalancing is due to fabrication imperfections meaning that the arms are not quite perfectly equal in length or that the metal for the heater slightly disturbs the optical mode. The power required to achieve the π phase change needed to switch the modulator from on to off is 17 mW, and the measured modulation depth is an impressive 20 dB. Fig. 4(b) also demonstrates the broadband nature of the modulator design—modulation is obtained over a bandwidth of 11 nm (marked by the dashed lines). In Fig. 4(d), the average transmission over this 11-nm bandwidth is plotted as a function of the electrical power. It is remarkable that the extinction ratio exceeds 15 dB over this whole range. In the current device, the insertion efficiency is relatively low—the insertion loss is measured to be 8–12 dB. This high value is a consequence of fabrication errors in the y-junction and photonic wires, and does not represent a limit to the design. In fact, the PhC phase shifters are expected to have a total loss of < 0.5 dB, given a loss per unit length in the flat-band slow-light region of the PhC phase shifters of 30–40 dB/cm [27].

Table 1 presents a comparison of the performance of our modulator device to other state-of-the-art PhC-based thermo-optic and electro-optic modulators [28], [29] and electro-optic modulators with conventional waveguide-based designs [4], [7].

With the exception of our device, the modulators in Table 1 use an unbalanced MZI configuration and thus the true bandwidth is not experimentally measured. We estimate that of [4] and [7] to be large, i.e., more than tens of nanometers, while [28] and [29] have very limited bandwidths due to the highly dispersive nature of the modes used.

4. Photonic Crystal Switch

4.1. Design and Fabrication

A directional coupler geometry is an alternate means of switching or modulating an optical signal. This consists of two identical waveguides placed in close proximity to one another. Slow light also offers significant enhancements to this device, and here, we show a PhC directional coupler that exhibits a very short coupling length and switching times as low as 3 ps.

Fig. 5 shows SEM images of the photonic crystal switch. The two PhC waveguides are placed sufficiently closely that the optical modes in each waveguide overlap and interact with each other. As with a conventional directional coupler, two supermodes are supported: one with even and the other with odd symmetry. Each mode has a different wave vector and therefore light in the system will couple from one waveguide to the other after a relative phase shift of π has occurred. This gives a switching length of $L = \pi/\Delta k$. Similar to the case of the dispersion-engineered modulator above, a large Δk is desirable to keep the switching length L small. The available change in refractive index is small and

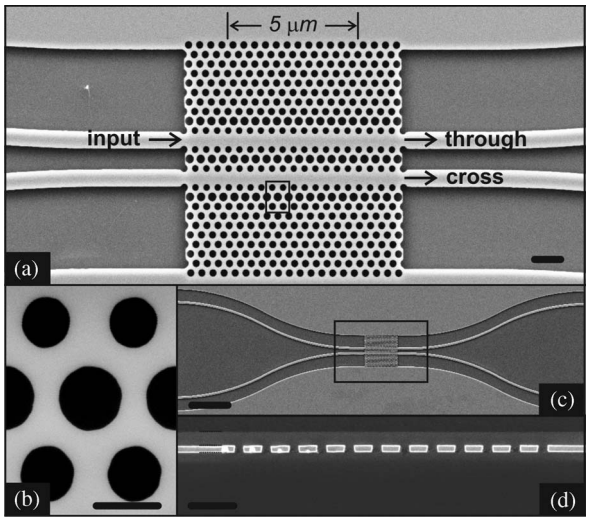

Fig. 5. (a)–(c) Scanning electron micrographs of the directional coupler switch. (a) The switch design is based on two closely spaced PhC waveguides in a directional-coupler geometry. Scale bar 1 μm. (b) Close-up of holes in the PhC. Scale bar 300 nm. (c) Overview of the chip layout. S-bends are used to separate the access waveguides. Scale bar 10 μm. (d) Cross section through the PhC switch after silica infilling. Scale bar 1 μm.

slow-light enhancement is necessary. Here, due to symmetry restrictions, we use a dispersion-engineering scheme following that of [22] and [30] and alter the sizes of the holes of the first two rows closest to the waveguide. Fig. 5 shows the design geometry. The resulting dispersion relation of the coupled modes in the central switch region is shown in Fig. 6(b). The design also includes mode conversion interface regions [10] with a slightly different dispersion to the switch region. These interfaces give a much improved coupling efficiency between the fast light of the input/output slab waveguides into/out of the engineered modes of the switch. This is achieved by increasing the lattice constant of the switch region along the direction of the waveguide only; see [10] for more details.

The PhC directional coupler switches are fabricated in the silicon-on-insulator similar to that of the modulator geometry described in Section 3.1; further details are available in [9] and [12].

4.2. Switch Performance

Using this design, we have demonstrated switching in a 5-μm-short device using a refractive index modulation of only $\Delta n = 4 \times 10^{-3}$, close to a 40-times reduction in length relative to conventional switches that operate with a similar Δn [28]. The total device area (including the interface regions) is just 10 μm $\times$ 10 μm, making it very useful for densely integrated networks. The insertion loss is comparable to that of the simple W1 photonic crystal waveguide—around 1 dB. The switch has a bandwidth of 1–2 nm, which compares favorably with switches and modulators based on cavity resonances—the competing means of realizing reduced footprint devices [8].

4.3. Ultrafast Measurements

To study the ultrafast dynamics of the switch, a pump–probe experiment was conducted. 100-fs duration pump pulses at a center wavelength of 800 nm and with a repetition rate of 80 MHz (provided by a Ti:Sapphire laser oscillator) were focused onto the silicon slab from above. The pumped area had an diameter of approximately 20 μm. The 800-nm wavelength radiation has an energy greater than that of the band gap of silicon and is absorbed, creating an electron-hole plasma that is homogeneous across the small dimensions of the device. Probe pulses with a center wavelength of 1486 nm (the operating wavelength of the switch) and a pulse duration of 2.8 ps (a bandwidth of 1.2 nm corresponding to the switching bandwidth) were used to measure the

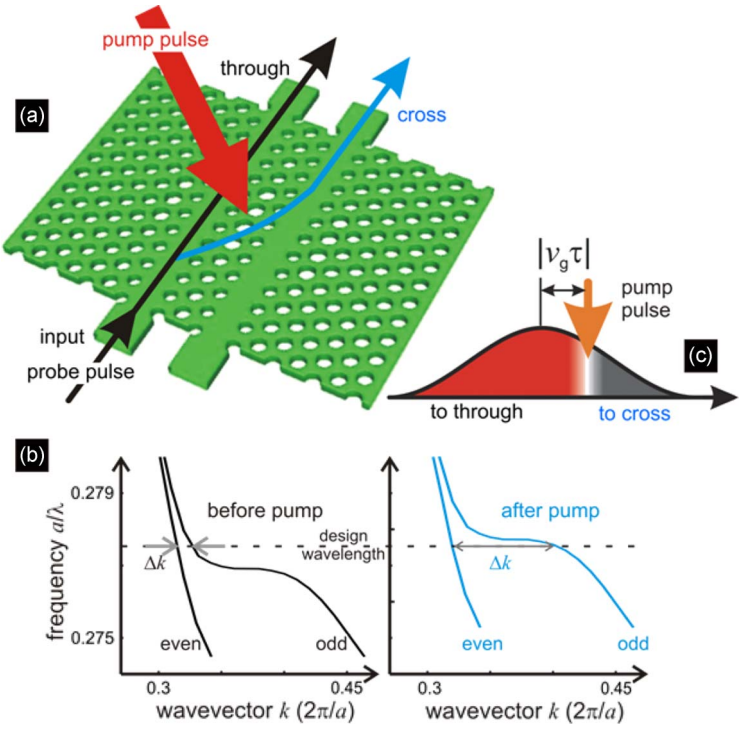

Fig. 6. (a) Schematic of the device and the pump–probe experimental setup. (b) Dispersion relation of the even and odd coupled supermodes of the device in the switching region, both before and after arrival of the pump pulse. (c) Rerouting process for delays around $\tau = 0$. Probe light that arrives before (after) the pump pulse exits the device at the through (cross) output ports.

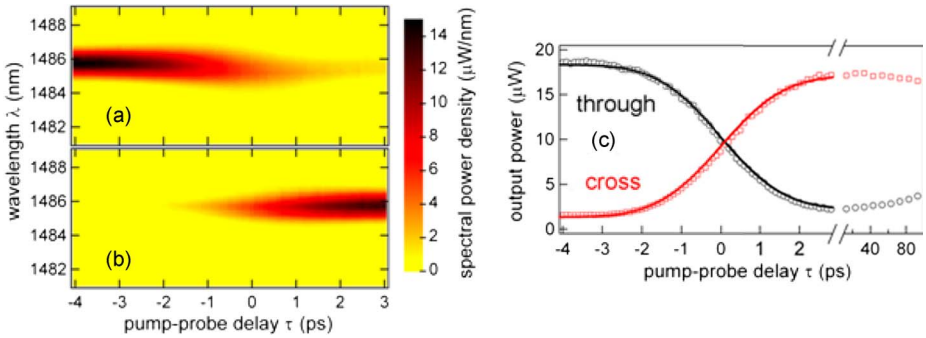

Fig. 7. Experimental data demonstrating the ultrafast rerouting of light. (a) The spectra of the probe pulses arriving at the through port as a function of the pump–probe delay time. (b) Similar spectra for the cross port. (c) Total power in the probe beam arriving at the through port (black circles) and cross port (red squares) as a function of τ. The lines are calculations based on eqs. (1) and (2).

instantaneous transmission from both the through and cross ports. The probe pulses are derived from the same laser source as the pump through the use of an optical parametric oscillator and a grating-based reflexive pulse shaper [31]. The probe pulses are then given a variable delay relative to the pump (with zero delay defined as the pump and probe arriving together at the center of the device) and coupled to the input port of the device. The transmitted probe pulse is collected by a lensed fiber at either the through or cross port and coupled into an OSA.

In Fig. 7(a) and (b), the probe intensity that reaches the through and cross ports, respectively, is shown as a function of the wavelength and the pump–probe delay. For delays < -2 ps, the device is

in its ground state when the probe pulse arrives, and it passes straight through the device to be collected at the through port. For delays > 2 ps, the pump pulse has already been incident on the device switching its state, resulting in the probe pulse being coupled into the cross port. Fig. 7(c) shows the total probe power arriving at the through and cross ports. Over 80% of the power is switched between ports in a window of less than 3 ps. The behavior of the device can be accurately modeled using

$$\text{through-port probe power} \propto \int_{\tau}^{\infty} I(t)dt \tag{1}$$

$$\text{cross-port probe power} \propto \int_{-\infty}^{\tau} I(t)dt \tag{2}$$

where $I(t)$ is the intensity of the incident 2.8-ps Gaussian probe pulse centered at $\tau = 0$. This comparison between experiment and theory leads to the conclusion that the 3-ps switching time is not given by the time of flight of the pulse through the device but is purely limited by the duration of the probe pulse. This in marked contrast to alternative (longer) designs [3], [32], [33] and originates in the cutting of the probe pulse into two separate pulses when τ is around zero, as illustrated in Fig. 6(c). Upon arrival of the pump pulse, the leading edge of the probe pulse has already exited the device via the through port. The trailing edge of the pulse is yet to enter the device, and will thus encounter the switching state and be directed to the cross port. The remaining part of the probe pulse (that part actually inside the switching region on arrival of the pump) can be neglected, as the transit time of the pulse (0.2 ps) is much smaller than its total duration (2.8 ps).

The longer time-scale dynamics of the device are also shown in Fig. 7. After a switching event, the switch takes approximately 400 ps to relax back to its ground state—very much longer than the 3-ps switching time. This relaxation time is governed by the time taken for the free carriers in the electron-hole plasma to recombine. This time could be shortened (for example) by placing the device in the middle of a $p-i-n$ diode. By applying a reverse bias, the generated free carriers could be "swept out," resulting in much shorter relaxation times.

5. Comparison

For silicon-based optical modulators to reach the small footprints required for optical interconnects, the weak refractive index changes available need significant enhancements. The recent plasmonic-based modulator of Dionne *et al.* [34] is an interesting development offering modulation with a very short, 2 μm, length though currently with prohibitive 20-dB loss. To date, the most popular and successful means of realizing this enhancement has been the use of high-Q micro ring resonators [6]. However, the high Q factor of the resonator is itself a major drawback, being very sensitive to thermal fluctuations and fabrication imperfections. Active compensation has been proposed as a solution, but this introduces a power consumption penalty. In [35], active compensation consumed up to 3 pJ/b at a bit rate of 1 Gb s^{-1}. While operation at higher bit rates should bring this number down, active compensation is still likely to consume more than the power budget available (for example, 0.097 pJ/b has been projected for 2015 from the ITRS 2007 roadmap [36]).

The need to avoid active compensation in devices targeting optical interconnect applications is thus a clear message. MZIs naturally give broad bandwidth operation even with small Δn. Chen *et al.* have used a slotted photonic crystal to reduce the device footprint achieving very low power consumptions, though with low bandwidth. The dispersion-engineered slow-light design described here, recovers sufficient bandwidth (11 nm) to give thermal insensitivity over a 100 °C range, for example, easily sufficient to cover the 55 °C fluctuations in microprocessor temperature during operating system boot-up reported in [37].

In future all-optical terahertz networks, performance, switching times and energies, may be expected to be the primary concern. High-Q micro ring resonators and photonic crystal cavities have been very successful in reducing switching energies to the sub-100-fJ range [38], but the

high Q factors used tend to limit the speed due to long photon lifetime (10s ps for $Q \approx 50\,000$). The bandwidth of the cavity is also insufficient to support the ultrashort < 5 ps pulses, which offer many advantages to these networks.

The PhC directional coupler switch provides an alternative to the high-Q approach. This design enhances the change in k-vector without actually slowing light down (see Fig. 6), resulting in a very short transit time (0.2 ps) through the device. This provides the potential for very fast operation. The relatively large bandwidth of the device ($\approx$1 nm) unavoidably requires a large Δn but readily supports picosecond pulses.

The recovery time remains an issue, though our value of 400 ps compares well with the 2 ns reported in [13]. This is a common issue and solutions such as ion implantation [38], and reverse biasing may be used. Alternatively, carriers may be allowed to recombine at the etched sidewalls of the photonic crystal holes offering a very convenient and fast $\sim$100-ps recovery mechanism [39]. The directional coupler switch also lends itself to the push–pull configuration in which a second switch is placed after the first and an additional control pulse is used to reroute the probe pulses back to the original path.

6. Conclusion

The design, fabrication, and characterization of a photonic crystal Mach–Zehnder optical modulator and a photonic crystal directional-coupler-based all-optical switch have been described. Both designs use the slow-light effect to provide resonant enhancement.

In the Mach–Zehnder modulator, flat-band slow-light photonic crystal waveguide phase shifters were placed in each arm with an integrated microheater used to actuate the device via the thermo-optic effect. The phase shifters exhibited a large group-index–bandwidth product allowing them to be just 80 μm long while still providing high extinction ratios over a large bandwidth. When combined with a *pn* diode, the small size of the PhC phase shifter will allow extremely small capacitances, enabling very high-speed operation.

The slow-light design of the directional coupler switch enabled a very short device length of just 5 μm. Ultrafast pump–probe measurements were used to demonstrate switching times as short as 3 ps. Due to the short transit time in the 5-μm device, the switching time is limited only by the duration of the input pulse. Therefore, the speed of the switch is bandwidth limited—faster switching times may only be shown by increasing the bandwidth of the device allowing the use of shorter probe pulses.

These two devices demonstrate slow light may enhance device performance and achieve ultracompact, low-power optical devices. As opposed to cavity-based solutions, slow-light enhancement provides an excellent compromise between size and switching power limitation on the one hand and bandwidth availability on the other. The designs are fully CMOS compatible and can be used with high-speed modulation approaches based on electro-optic effects to offer very exciting performance enhancements.

References

[1] G. T. Reed and C. B. J. Png, "Silicon optical modulators," *Mater. Today*, vol. 8, no. 1, pp. 40–50, Jan. 2005.
[2] G. T. Reed, "The optical age of silicon," *Nature*, vol. 427, no. 6975, pp. 595–596, Feb. 2004.
[3] V. R. Almeida, C. A. Barrios, R. R. Panepucci, and M. Lipson, "All-optical control of light on a silicon chip," *Nature*, vol. 431, no. 7012, pp. 1081–1084, Oct. 2004.
[4] A. Liu, L. Liao, D. Rubin, H. Nguyen, B. Ciftcioglu, Y. Chetrit, N. Izhaky, and M. Panicca, "High-speed optical modulation based on carrier depletion in a silicon waveguide," *Opt. Express*, vol. 15, no. 2, pp. 660–668, Jan. 2007.
[5] A. Liu, R. Jones, L. Liao, D. Samara-Rubio, D. Rubin, O. Cohen, R. Nicolaescu, and M. Paniccia, "A high speed silicon optical modulator based on a metal-oxide-semiconductor capacitor," *Nature*, vol. 427, no. 6975, pp. 615–618, Feb. 2004.
[6] Q. Xu, B. Schmidt, S. Pradhan, and M. Lipson, "Micrometre-scale silicon electro-optic modulator," *Nature*, vol. 435, no. 7040, pp. 325–327, May 2005.
[7] W. M. J. Green, M. J. Rooks, L. Sekaric, and Y. A. Vlasov, "Ultra-compact, low RF power, 10 Gb/s silicon Mach–Zehnder modulator," *Opt. Express*, vol. 15, no. 25, pp. 17 106–17 113, Dec. 2007.
[8] M. Notomi, A. Shinya, S. Mitsugi, G. Kira, B. Kuramochi, and T. Tanabe, "Optical bistable switching action of Si high-q photonic-crystal nanocavities," *Opt. Express*, vol. 13, no. 7, pp. 2678–2687, Apr. 2005.
[9] D. M. Beggs, T. P. White, L. O'Faolain, and T. F. Krauss, "Ultracompact and low power optical switch based on silicon photonic crystals," *Opt. Lett.*, vol. 33, no. 2, pp. 147–149, Jan. 2008.

[10] S. Schulz, L. O'Faolain, D. M. Beggs, T. White, and T. F. Krauss, "Dispersion free slow light in photonic crystals: A comparison," *J. Opt.*, in press.
[11] E. A. Camargo, H. M. H. Chong, and R. M. De La Rue, "2D Photonic crystal thermo-optic switch based on AlGaAs/GaAs epitaxial structure," *Opt. Express*, vol. 12, no. 4, pp. 588–592, Feb. 2004.
[12] D. M. Beggs, T. P. White, L. Cairns, L. O'Faolain, and T. F. Krauss, "Ultrashort photonic crystal optical switch actuated by a microheater," *IEEE Photon. Technol. Lett.*, vol. 21, no. 1, pp. 24–26, Jan. 2009.
[13] Y. Vlasov, W. M. J. Green, and F. Xia, "High-throughput silicon nanophotonic wavelength-insensitive switch for on-chip optical networks," *Nat. Photon.*, vol. 2, no. 4, pp. 242–246, Apr. 2008.
[14] T. Kampfrath, D. M. Beggs, T. P. White, M. Burresi, D. Oosten, T. F. Krauss, and L. Kuipers, "Ultrafast re-routing of light via slow modes in a nano-photonic directional coupler," *Appl. Phys. Lett.*, vol. 94, no. 24, p. 241 119, Jun. 2009.
[15] T. Kampfrath, D. M. Beggs, T. F. Krauss, and L. Kuipers, "Full characterization of ultrafast nano-photonic devices," *Opt. Lett.*, vol. 34, pp. 3418–3420, 2009.
[16] F. Gardes, A. Brimont, P. Sanchis, G. Rasigade, D. Marris-Morini, L. O'Faolain, F. Dong, J. Fedeli, P. Dumon, L. Vivien, T. Krauss, G. Reed, and J. Marti, "High-speed modulation of a compact silicon ring resonator based on a reverse-biased pn diode," *Opt. Express*, vol. 17, no. 24, pp. 21 986–21 991, Nov. 2009.
[17] A. Gomez-Iglesias, D. O'Brien, L. O'Faolain, A. Miller, and T. F. Krauss, "Direct measurement of the group index of photonic crystal waveguides via Fourier transform spectral interferometry," *Appl. Phys. Lett.*, vol. 90, no. 26, p. 261 107, Jun. 2007.
[18] A. Petrov and M. Eich, "Zero dispersion at small group velocities in photonic crystal waveguides," *Appl. Phys. Lett.*, vol. 85, no. 21, pp. 4866–4868, Nov. 2004.
[19] M. D. Settle, R. J. P. Engelen, M. Salib, A. Michaeli, L. Kuipers, and T. F. Krauss, "Flatband slow light in photonic crystals featuring spatial pulse compression and terahertz bandwidth," *Opt. Express*, vol. 15, no. 1, pp. 219–226, Jan. 2007.
[20] J. Li, T. P. White, L. O'Faolain, A. Gomez-Iglesias, and T. F. Krauss, "Systematic design of flat band slow light in photonic crystal waveguides," *Opt. Express*, vol. 16, no. 9, pp. 6227–6232, Apr. 2008.
[21] J. M. Brosi, J. Leuthold, and W. Freude, "Microwave-frequency experiments validate optical simulation tools and demonstrate novel dispersion-tailored photonic crystal waveguides," *J. Lightw. Technol.*, vol. 25, no. 9, pp. 2502–2510, Sep. 2007.
[22] L. H. Frandsen, A. V. Lavrinenko, J. Fage-Pedersen, and P. I. Borel, "Photonic crystal waveguides with semi-slow light and tailored dispersion properties," *Opt. Express*, vol. 14, no. 20, pp. 9444–9450, Oct. 2006.
[23] S. Kubo, D. Mori, and T. Baba, "Low-group-velocity and low-dispersion slow light in photonic crystal waveguides," *Opt. Lett.*, vol. 32, no. 20, pp. 2981–2983, Oct. 2007.
[24] D. Mori and T. Baba, "Wideband and low dispersion slow light by chirped photonic crystal coupled waveguide," *Opt. Express*, vol. 13, no. 23, pp. 9398–9408, Nov. 2005.
[25] D. M. Beggs, L. O'Faolain, and T. F. Krauss, "Accurate determination of the functional hole size in photonic crystal slabs using optical methods," *Photon. Nanostructures: Fundam. Appl.*, vol. 6, no. 3/4, pp. 213–218, Dec. 2008.
[26] T. P. White, L. O'Faolain, J. Li, L. C. Andreani, and T. F. Krauss, "Silica-embedded silicon photonic crystal waveguides," *Opt. Express*, vol. 16, no. 21, pp. 17 076–17 081, Oct. 2008.
[27] L. O'Faolain, S. Schulz, D. M. Beggs, T. P. White, A. D. Falco, A. Samarelli, M. Sorel, R. M. De La Rue, F. Morichetti, A. Canciamilla, A. Melloni, and T. F. Krauss, "Low loss dispersion engineered photonic crystal waveguides for optical delay lines," in *Proc. 6th IEEE Int. Conf. Group IV Photon.*, 2009, pp. 40–42.
[28] Y. A. Vlasov, M. O'Boyle, H. F. Hamann, and S. J. McNab, "Active control of slow light on a chip with photonic crystal waveguides," *Nature*, vol. 438, no. 7064, pp. 65–69, Nov. 2005.
[29] X. Chen, Y.-S. Chen, Y. Zhao, W. Jiang, and R. T. Chen, "Capacitor-embedded 0.54 pJ/bit silicon-slot photonic crystal waveguide modulator," *Opt. Lett.*, vol. 34, no. 5, pp. 602–604, Mar. 2009.
[30] N. Yamamoto, T. Ogawa, and K. Komori, "Photonic crystal directional coupler switch with small switching length and wide bandwidth," *Opt. Express*, vol. 14, no. 3, pp. 1223–1229, Feb. 2006.
[31] R. Nelson, D. Leaird, and A. Weiner, "Programmable polarization-independent spectral phase compensation and pulse shaping," *Opt. Express*, vol. 11, no. 15, pp. 1763–1769, Jul. 2003.
[32] M. Waldow, T. Plotzing, M. Gottheil, M. Forst, J. Bolten, T. Wahlbrink, and H. Kurz, "25 ps all-optical switching in oxygen implanted silicon-on-insulator microring resonator," *Opt. Express*, vol. 16, no. 11, pp. 7693–7702, May 2008.
[33] H. Nakamura, Y. Sugimoto, K. Kanamoto, N. Ikeda, Y. Tanaka, Y. Nakamura, S. Ohkouchi, Y. Watanabe, K. Inoue, H. Ishikawa, and K. Asakawa, "Ultra-fast photonic crystal/quantum dot all-optical switch for future photonic networks," *Opt. Express*, vol. 12, no. 26, pp. 6606–6614, Dec. 2004.
[34] J. A. Dionne, K. Diest, L. A. Sweatlock, and H. A. Atwater, "Plasmostor: A metal-oxide-Si field effect plasmonic modulator," *Nano Lett.*, vol. 9, no. 2, pp. 897–902, Feb. 2009.
[35] S. Manipatruni, R. K. Dokania, B. Schmidt, N. Sherwood-Droz, C. B. Poitras, A. B. Apsel, and M. Lipson, "Wide temperature range operation of micrometer scale silicon electro-optic modulators," *Opt. Lett.*, vol. 33, no. 19, pp. 2185–2187, Oct. 2008.
[36] D. A. B. Miller, "Device requirements for optical interconnects to silicon chips," *Proc. IEEE*, vol. 97, no. 7, pp. 1166–1185, Jul. 2009.
[37] H. F. Hamann, A. Weger, J. A. Lacey, Z. Hu, P. Bose, B. Cohen, and J. Wakil, "Hotspot-limited microprocessors: Direct temperature and power distribution measurements," *IEEE J. Solid-State Circuits*, vol. 42, no. 1, pp. 56–65, Jan. 2007.
[38] T. Tanabe, K. Nishiguchi, A. Shinya, E. Kuramochi, H. Inokawa, and M. Notomi, "Fast all-optical switching using ion-implanted silicon photonic crystal nanocavities," *Appl. Phys. Lett.*, vol. 90, no. 3, p. 031 115, Jan. 2007.
[39] T. Tanabe, M. Notomi, S. Mitsugi, A. Shinya, and E. Kuramochi, "All-optical switches on a silicon chip realized using photonic crystal nanocavities," *Appl. Phys. Lett.*, vol. 87, no. 15, p. 151 112, Oct. 2005.